Applied Thermal Engineering 241 (2024) 122340

Contents lists available at ScienceDirect

Applied Thermal Engineering

journal homepage: www.elsevier.com/locate/apthermeng

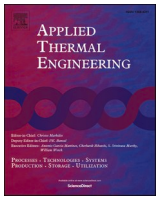

Research Paper

Quasi-2D thermal network based heat soakage model for gas turbine transient performance modification

Yimin Yang *, Theoklis Nikolaidis, Pericles Pilidis

Centre for Propulsion and Thermal Power Engineering, School of Aerospace Transport and Manufacturing (SATM), Cranfield University, Cranfield, Bedfordshire, MK43 0AL, UK

ARTICLE INFO

Keywords:
Gas Turbine Transient
Heat Soakage Effect
Quasi-2D Thermal Network
Performance Simulation
Response Delay

ABSTRACT

To overcome the limitations of traditional heat soakage analysis, a novel quasi-2D thermal network based heat soakage model is established with the consideration of component internal thermal resistance, combustor temperature profile, cooling technologies and thermal barrier coating. The method has been integrated into Turbomatch, a gas turbine performance software developed by Cranfield University, to offer a more realistic estimation of the heat soakage effect during the gas turbine transient manoeuvre. The accuracy of the heat soakage model has been validated against results obtained from GasTurb. Furthermore, a parametric analysis has been conducted to evaluate the effects of combustor temperature profile, cooling technologies, and thermal barrier coating. It is found that the combustor temperature profile will cause a significant increase in heat flow rate, which is approximately four times the conventional lumped parameter method based model. The implementation of cooling technologies and thermal barrier coating will reduce the heat flow rate by 48.97%. More importantly, the change in heat flow rate causes a further delay in engine transient response. Corrected rotational speed was decreased by 0.89%, and thrust was reduced by 2.24%. Moreover, a delay of 8s (233% increase) in the transient acceleration time was found when comparing the quasi-2D thermal network based heat soakage model with the traditional lumped parameter method based model. These highlight the significance of accurately evaluating the heat soakage effects during gas turbine transient simulation.

1. Introduction

Gas turbine performance simulation, especially its transient part, has become an increasingly valuable tool for engine design. Over the past 70 years, several transient simulation methodologies have been developed, including the constant mass flow (CMF) method [1], inter-component volume method [2], pressure wave in volume method [3] and imbalanced mass flow method [4]. However, ongoing research on gas turbine transient performance prediction has revealed discrepancies between simulation and experimental results [5]. This has led to the identification of additional factors that affect engine transient operation, such as the heat soakage effect.

When analyzing the steady-state performance of an engine, it is reasonable to assume that the compression and expansion process occurs adiabatically, as the heat flows are negligible when gas turbine is under thermal equilibrium (steady-state) condition. However, significant heat is transferred between the primary gas path and the engine's metal components during transient manoeuvres, which cannot be ignored. This heat transfer leads to energy losses, and it typically requires an additional 30 % of fuel energy to reach a new, higher steady-state operating temperature [6].

Many researchers have included this phenomenon in their research to investigate the impact of heat soakage. A comprehensive review related to heat soakage has been done by the author [7]. A brief literature review will be shown here. Maccallum studied the non-adiabatic compression and expansion process caused by the heat soakage effect [8]. He modified the index of compression and expansion based on the heat flow between the engine metal and the working gas. It was found that the additional heat flow from the engine metal to the air led to an increase in the specific heat (*Cp*). The lumped parameter method (LPM) has been widely utilized for heat soakage analysis due to its convenience [9–14]. In the LPM, each component is assumed as a mass node at the centre of real component geometry. The mass node temperature represents the temperature of the whole component, so the internal heat conduction is neglected. Besides, the fluid temperature is kept constant during the heat transfer process, which would lead to an overestimation of the heat transfer rate. Khalid and Hearne were among the first to

* Corresponding author.
E-mail address: yimin.yang96@cranfield.ac.uk (Y. Yang).

https://doi.org/10.1016/j.applthermaleng.2024.122340
Received 29 August 2023; Received in revised form 27 November 2023; Accepted 2 January 2024
Available online 6 January 2024

Nomenclature:

A	Area (m^2)
APR	Aspect Ratio
CFM	Constant Mass Flow
CN	Corrected Rotational Speed (%)
Cp	specific heat (J/kg K)
CVM	Control Volume Method
D	Diameter (m)
FAR	Fuel to Air Ratio
h	Height (m), Heat Transfer Coefficient (W/m^2/K)
HTC	Heat Transfer Coefficient
L	Length (m)
LHV	Lower Heating Value (MJ/kg)
LPM	Lumped Parameter Method
M	Mass (kg)
Mach	Mach Number
N	Number
P	Stagnation Pressure (Pa)
PCR	Pitch/Chord Ratio
Q	Flow Function, Quantity of Heat (W)
R	Gas Constant (J/kg K)
SL	Stage Length (m)
T	Stagnation Temperature (K)
t	Time (s)
TBC	Thermal Barrier Coating
TDM	Temperature Difference Method
Th	Thickness (m)
TM	TURBOMATCH
W	Mass Flow (kg/s)
x	Distance (m)
2D	2-Dimensional

Greek letters

Φ	Heat flow rate (kW)
τ	Time Constant
λ	Conductive Coefficient (W/(m K))
σ	Stefan-Boltzmann Constant (W/(m^2 K^4))
ε	Emissivity
η	Efficiency
ν	Viscosity (m^2/s)
ρ	Density (kg/m^3)
γ	Ratio of Specific Heats

Subscript

b	Blade
c	Casing
D	Difference
d	Disc
f	Fluid
ft	Flame Tube
g	Gas
h	Hub
m	Mean, Metal
t	Tip
w	Wall

Postscript

i	Transient Calculation Time Step

employ the LPM to estimate the heat soakage effect on gas turbine transient performance [9]. However, they assumed a constant heat transfer coefficient (HTC) during transient maneuvers. Zhili et al. improved HTC estimation by introducing a more realistic boundary development model [12]. However, they did not address the limitation of the LPM discussed above. Qiuye et al. applied a similar method, and the authors considered the effect of film cooling and thermal barrier coating (TBC) on turbine blade wall temperature [10]. However, instead of establishing a physical-based model, they simplified the TBC model as a temperature reduction on the blade wall temperature. Visser et al. established a LPM based thermal network for Gas Turbine Simulation Program heat soakage simulation [13]. The accuracy of the heat soakage model was compared with experiment data, but there was a relatively large difference. Vieweg et al. developed a heat soakage model based on LPM. They compared their results with experimental data and an improvement in model accuracy was found when compared with the model without considering the heat soakage effect [11,14]. However, improvements can be made to consider cooling technologies and heat conduction. Naylor developed the stream method for the disc heat soakage estimation [15]. In the stream method, the disc was divided into several blocks. Based on this, a complex geometry and conductive heat transfer process could be considered in contrast to the LPM. Kypuros et al. established a 1-D analytical method for turbine disc axial direction temperature estimation [16,17]. Both convection and conduction heat transfer processes were considered. Chapman et al. improved Kypuros's model into the finite element method to predict the axial disc temperature based on the disc cooling flow temperature [18,19]. Nevertheless, they both neglected the heat flow from the main gas path. Fengping et al. developed a quasi-1-dimensional thermal network that considered each stage of components based on the LPM [20]. Zhuojun developed a 1-D thermal network in the gas turbine axial direction [21]. Ferrand et al. investigated power losses due to heat soakage in a reverse-flow combustor [22]. The author mentioned that heat soakage modelling in the combustion chamber alone was not sufficient to correct the gas generator speed trajectory.

Based on the literature review, the following research gaps have been identified in the modelling of heat soakage in gas turbine transient simulation:

1. Traditional LPM lacks the consideration of fluid temperature change during the heat transfer process[9–14].
2. The component internal thermal resistance was lack of investigation [9–14,16–22].
3. The combustor heat soakage model does not take into account the consideration of axial temperature profile or is even neglected during the heat soakage investigation [9–22].
4. Cooling technologies such as film cooling, TBC and internal cooling were often neglected or simplified[9–22].

The current research presented here addresses these gaps including:

1. The development of a temperature difference method (TDM) that considers the change of gas temperature per time step during the transient phase improves the LPM against the constant value used so far.
2. The development of a control volume method (CVM) offers a more accurate heat transfer process estimation by considering component internal temperature distribution.
3. The development of the combustor heat soakage model with the introduction of temperature profile in the axial direction, encompassing the primary zone, secondary zone, and dilution zone, offers a more realistic combustor heat transfer estimation.

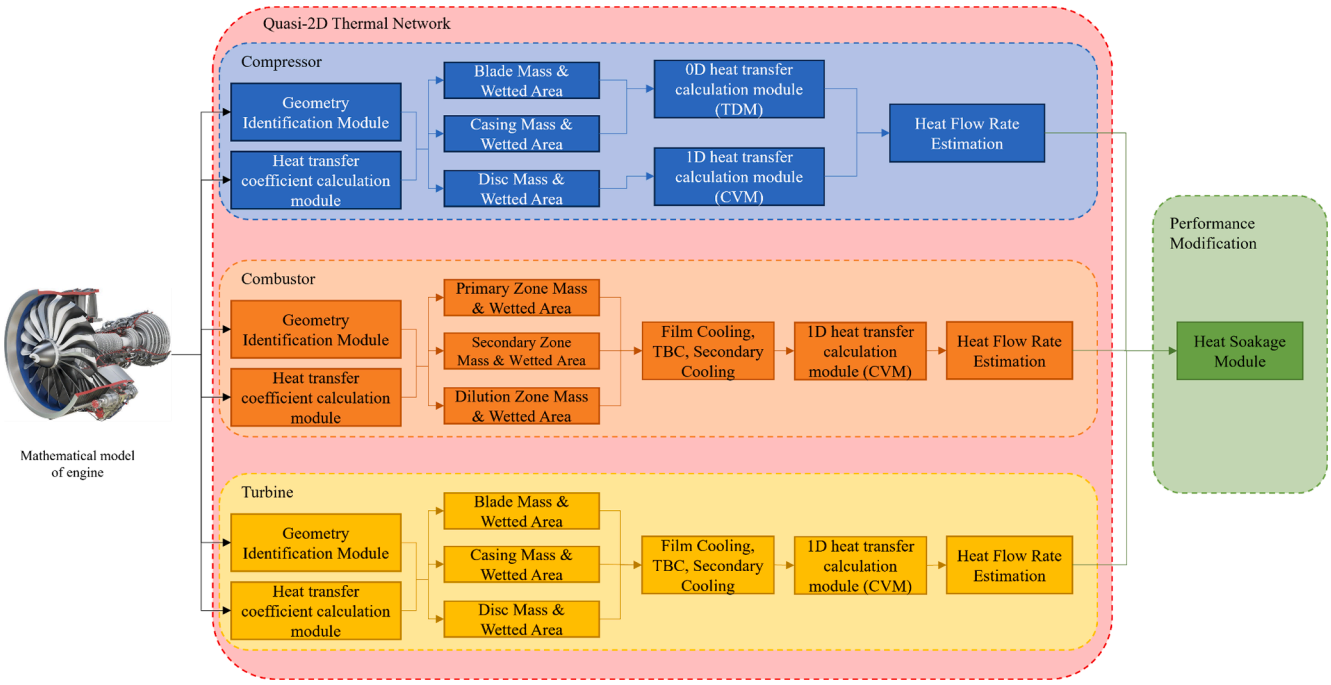

Fig. 1. Heat soakage model calculation logic.

4. The inclusion of cooling effects for the combustor and turbine, modelling the impact of cooling technology such as TBC, film cooling, and internal cooling improves the heat transfer estimation.

The above models are implemented in a quasi-2D thermal network based heat soakage model, which provides a more realistic simulation of the heat soakage effects on gas turbine engines.

The paper is structured in the following way:

Firstly, the underlying physical principles of heat soakage in gas turbine components are studied. The methodology of the proposed heat soakage model is described. The focus is on the three key engine components: the compressor, combustor, and turbine. Each component has its specific heat transfer processes, including convective, conductive, and radiative heat transfer.

Secondly, a gas turbine dynamic model incorporating the heat soakage model is developed. Its results are compared for validation with those obtained from the commercial software GasTurb.

Finally, the effect of the combustor temperature profile and several cooling technologies is investigated by comparing the outcome with the LPM model. The analysis illustrates the significance of their impact on gas turbine transient performance.

Overall, this research offers valuable insights into modelling heat soakage in gas turbine components, presents a validated dynamic model, and explores the effects of different features within the proposed heat soakage model on gas turbine transient performance.

2. Modelling method of heat soakage model

The establishment of the heat soakage model includes two essential steps: quasi-2D thermal network establishment (including geometry identification and heat flow rate estimation) and component performance modification. The workflow chart of heat soakage model is presented in Fig. 1.

2.1. Quasi-2D thermal network

Quasi-2D thermal network includes two essential parts, the first is the component geometry identification and the second is the heat flow rate calculation. Based on these two parts, the thermal network can be established.

2.1.1. Component geometry identification

The heat soakage effect is strongly related to the geometry of the components, as it will affect the components' mass, wetted area, and heat transfer coefficient. The change in component geometry will lead to a variation in heat transfer rate during transient and further effect the gas turbine transient performance. During component geometry identification, three components are considered: the compressor, combustor, and turbine. Since compressor and turbine have the similar geometry, they will be discussed together in Section 2.1.1.1. And the combustor geometry identification method will be discussed in Section 2.1.1.2.

2.1.1.1. Compressor and turbine geometry identification method. During the preliminary design process for the compressor and turbine, it is assumed that (1) stage temperature rise or drop is kept constant; (2) the axial flow velocity at each stage inlet position is kept constant; (3) the compressor and turbine consist of three parts: blades, casing, and disc; (4) the annulus shape of the compressor and turbine are simplified into three types: constant hub diameter, constant tip diameter, and constant mean diameter.

The annulus areas of the compressor and turbine at different stages are determined by the flow function Q in Eqs.(1) [23], where $Mach$ is the axial Mach number at each stage inlet position, γ is ratio of specific heats, R is gas constant. With flow function Q the flow area can be obtained by Eqs. (2), where A is area, W is mass flow, T is stagnation temperature, K_B is compressor inlet blockage factor and P is stagnation pressure.

$$Q = Mach \cdot \sqrt{\frac{\gamma}{R}} \cdot \left(1 + \frac{\gamma - 1}{2} Mach^2\right)^{\left(\frac{-(\gamma+1)}{2(\gamma-1)}\right)} \tag{1}$$

$$A = \frac{W\sqrt{T}}{K_B P Q} \tag{2}$$

The tip diameter (D_t), hub diameter (D_h), and mean diameter (D_m) at the inlet of the compressor and turbine are estimated using the design inlet

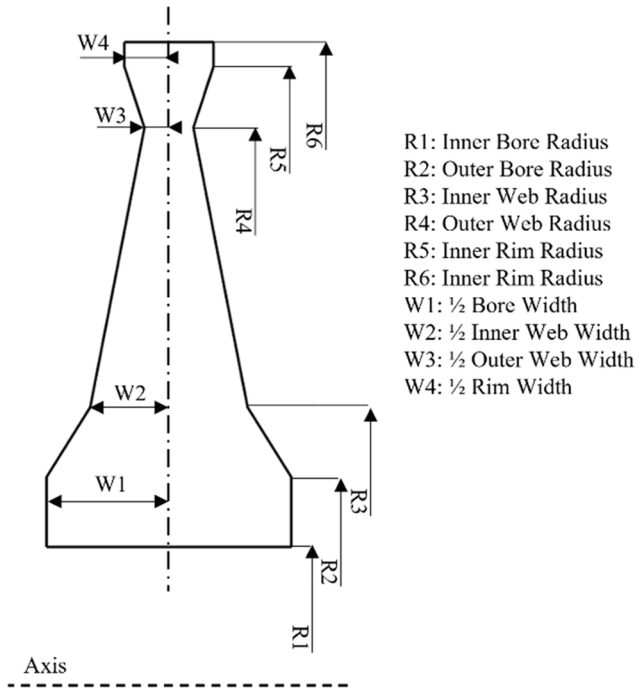

Fig. 2. Parameterized disc model.

hub-to-tip ratio and estimated flow area A during the preliminary design process. Then, based on the selected compressor type, each stage's tip and hub diameter can be determined. The number of blades for each stage will be estimated by using the design aspect ratio and pitch/chord ratio, which is shown in Eqs. (3) [24], where N_b is the blade number, h_b is blade hight, APR is aspect ratio and PCR is pitch/chord ratio.

$$N_b = \pi \cdot \frac{(D_t + D_h)}{2} / (h_b / APR \cdot PCR) \tag{3}$$

When estimating the mass and wetted area, the blades are assumed to be flat plates, the casings are assumed to be hollow cylinders and discs are assumed to be hollow cylinder with certain shape. The parameters used to define disc profile are shown in Fig. 2.

These assumptions allow for straightforward calculations of each component's volume and wetted area. Once the material density is known, the mass can be estimated. Related equations are listed in Eqs. (4)–(9), where A is the wetted area of each component part, SL is the stage axial length, Th is the thickness of component, M is the mass of of each component part and ρ is the density of the material.

$$A_b = N_b \cdot 2 \cdot h_b \cdot Chord_b \tag{4}$$

$$A_c = \pi \cdot D_t \cdot SL \tag{5}$$

$$A_d = \pi \cdot D_h \cdot SL \tag{6}$$

$$M_b = A_b \cdot Th_b \cdot \rho_b / 2 \tag{7}$$

$$M_c = A_c \cdot Th_c \cdot \rho_c \tag{8}$$

$$M_d = f(Radius, Width, \rho_d) \tag{9}$$

2.1.1.2. Combustor geometry identification method. During the combustor preliminary design, the outer casing of the combustor will not be considered since it will not directly contact the high-temperature flame. Only the flame tube will be considered during the combustor preliminary design. Three types of combustors are considered: tubular combustor, tubo-annular combustor, and annular combustor.

The combustor reference area will be calculated by using Eqs. (10),

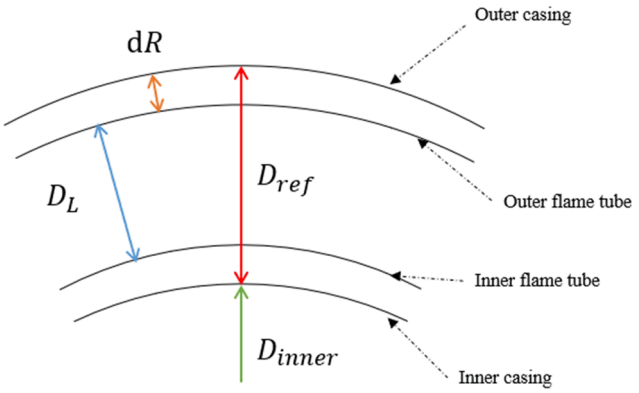

Fig. 3. Structure illustration of annular combustor.

where $\frac{\Delta P_{3-4}}{q_{ref}}$ is the pressure drop factor (PDF), ΔP_{3-4} is the pressure loss [25].

$$A_{ref} = \left(\frac{R}{2} \left(\frac{W_3 \cdot \sqrt{T_3}}{P_3} \right)^2 \cdot \frac{\Delta P_{3-4}}{q_{ref}} \cdot \left(\frac{\Delta P_{3-4}}{P_3} \right)^{-1} \right)^{0.5} \tag{10}$$

PDF's value varies for different types of combustors [25]. For the tubular combustor, the PDF is 37; for the tubo-annular combustor, it is 28; and for the annular combustor, it is 20.

With the estimated reference area, Eqs. (11) will be applied to estimate the liner area of the combustor, as we are only considering the flame tube instead of the entire combustor. Eqs. (12) will be used to estimate the tubular and tubo-annular flame tube diameter.

$$A_L = 0.66 \cdot A_{ref} \tag{11}$$

$$D_{tube} = \sqrt{A_L \cdot 4 / (N_{tube} \cdot \pi)} \tag{12}$$

For the annular combustor, the structure is illustrated in Fig. 3. Since the area is between two hollow cylinders, we need to calculate the outer and inner diameter of the cylinder by using $dR = (D_{ref} - D_L)/2$. The equations used for estimation are listed in Eqs. (13)–(16).

$$D_{ref} = \left(\sqrt{4 \cdot A_{ref} / \pi + D_{inner}^2} - D_{inner} \right) \Big/ 2 \tag{13}$$

$$dR = \left(D_{outer}^2 - D_{inner}^2 - 4 \cdot A_L / \pi \right) / \left(8 \cdot (D_{outer} + D_{inner}) \right) \tag{14}$$

$$D_{ft\_outer} = D_{outer} - 2 \cdot dR \tag{15}$$

$$D_{ft\_inner} = D_{inner} + 2 \cdot dR \tag{16}$$

The flame tube is approximated as a hollow cylinder when estimating the mass and wetted area. The mass and wetted area can be estimated by using Eqs. (17)–(18), where L is the axial length of the combustor.

$$A_{burner} = \pi \cdot (D_{ft_{outer}} + D_{ft\_inner}) \cdot L_{burner} \tag{17}$$

$$M_{burner} = A_{burner} \cdot Th_{burner} \cdot \rho_{burner} \tag{18}$$

2.1.2. Component heat flow rate estimation

Based on the geometry identification method described in Section 2.1.1, the heat flow rate between the working fluid and the component metal can be estimated. To address the research gap outlined in Section 1, various heat transfer models have been developed. In this section, two types of fundamental heat transfer models will be discussed. The first is the TDM, which is suitable for low Biot number component parts, such as compressor blades and casings. The second is the CVM, which is suitable for high Biot number component parts, including compressor discs, combustor flame tubes, turbine blades, casings, and discs.

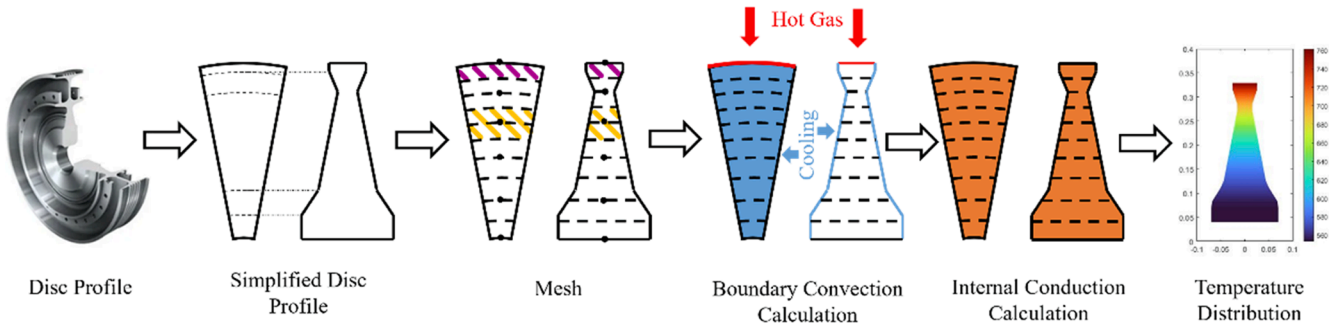

Fig. 4. CVM calculation process (turbine disc as an example).

2.1.2.1. Temperature difference method. For compressor blades and casing, the Biot number, which is the ratio of thermal-conduction resistance to the heat transfer resistance on the unit area, is relatively low (Bi < 1) [26]. Thus, their conduction resistance is much smaller than the heat convection at the surface. It can be assumed that the temperature gradients inside them are negligible and have an even temperature distribution. Under this assumption, the LPM can be applied, which assumes that the temperature field inside the component is uniform and treats the component as a mass node located at the centre of the component and surrounded by the fluid. However, the traditional LPM assumes constant fluid temperature during the heat transfer process, which can introduce errors. To address this, the TDM is developed to include changes in fluid temperature.

Given the wetted area, heat transfer coefficient, fluid temperature, and mass temperature, the heat flow rate between the fluid and the mass can be estimated using Eqs. (19), where Φ is the heat flow rate, $\boldsymbol{h}$ is the heat transfer coefficient, $\boldsymbol{T_g}$ is the gas stagnation temperature and $\boldsymbol{T_m}$ is the metal temperature. This heat flow rate can then be used to estimate the temperature change rate using Eqs. (20), where $\boldsymbol{Cp}$ is the specific heat and $\boldsymbol{t}$ is time. Let $\boldsymbol{T_D} = \boldsymbol{T_g} - \boldsymbol{T_m}$, where both $\boldsymbol{T_g}$ and $\boldsymbol{T_m}$ are function of time, so $\boldsymbol{T_D}$ is also a function of time. Based on this, we can get $\boldsymbol{dT_D} = \boldsymbol{dT_g} - \boldsymbol{dT_m}$.

Combining Eqs. (19) and Eqs. (20), Eqs. (21) can be derive, which represents the new temperature difference between fluid and mass after a time period Δt. Let a time constant $\tau = \frac{h \cdot A}{M_m \cdot Cp_m} + \frac{h \cdot A}{M_f \cdot Cp_f}$, then the quantity of heat transfer between fluid and mass in a certain time period Δt can be obtained by Eqs. (22), where $\boldsymbol{Q}$ is the quantity of heat. The temperature of fluid and mass at the end of this time period can be estimated based on the estimated quantity of heat by Eqs. (23). The thermal properties for gas and metal are listed in Appendix A.

$$\Phi = \boldsymbol{h} \cdot \boldsymbol{A} \cdot \left(\boldsymbol{T_g} - \boldsymbol{T_m} \right) \tag{19}$$

$$\Phi = \boldsymbol{M_m} \cdot \boldsymbol{Cp_m} \cdot \left(\frac{d\boldsymbol{T_m}}{dt} \right) = -\boldsymbol{M_f} \cdot \boldsymbol{Cp_f} \cdot \left(\frac{d\boldsymbol{T_f}}{dt} \right) \tag{20}$$

$$\boldsymbol{T_D} = \boldsymbol{T_{D0}} \cdot \boldsymbol{e}^{-\left(\frac{h \cdot A}{M_m \cdot Cp_m} + \frac{h \cdot A}{M_f \cdot Cp_f} \right) \Delta t} \tag{21}$$

$$\boldsymbol{Q} = \int_0^{\Delta t} \Phi dt = -\boldsymbol{h} \cdot \boldsymbol{A} \cdot \left(\boldsymbol{T_{g0}} - \boldsymbol{T_{m0}} \right) \cdot \frac{1}{\boldsymbol{\tau}} \cdot \left(\boldsymbol{e}^{-\tau \Delta t} - 1 \right) \tag{22}$$

$$\boldsymbol{T_t} = \boldsymbol{T_0} + \frac{\boldsymbol{Q}}{\boldsymbol{M} \cdot \boldsymbol{Cp}} \tag{23}$$

2.1.2.2. Control volume method. The proposed TDM is suitable for low Biot Number components. However, for those with a non-uniform temperature distribution (such as compressor discs, combustor flame tubes, turbine blades, casings, and discs), TDM becomes unsuitable. It is necessary to employ a more fitting model for these components. In order to determine the temperature distribution within such components, the CVM is developed. The calculation process of the CVM is illustrated in Fig. 4, using the turbine disc as an example. In this section, the calculation process of the CVM will be discussed, covering component geometry feature capture, mesh, initial conditions, boundary conditions, and numerical solving.

A. Component Geometry Feature Capture and Mesh

Five components are considered when applying the CVM, which are compressor disc, combustor flame tube, and turbine blade, casing and disc. According to Section 2.1, the blade is modelled as a flat plate, combustor flame tube, and casing are simplified as hollow cylinders, and the disc is represented as a hollow cylinder with a specific shape.

For the turbine blade, part of the blade wall (highlighted in the red box in Fig. 5 (a), Step 2) is chosen as the analyzed part, as it allows for the capture of film cooling, internal convective cooling, and TBC. Meshing is performed in the blade thickness direction. Regarding the combustor flame tube and turbine casing, the wall (highlighted in the red box in Fig. 5 (b), Step 2) is selected as the analyzed part, with meshing in the radius direction. For the disc, the cross-sectional area is chosen as the analyzed part, with meshing also in the radius direction, as shown in Fig. 5 (c). Additionally, the simulation of TBC involved the use of additional layers of mesh, as depicted in Fig. 5 (d).

An example of the resulting mesh is shown in Fig. 6. In the figure, the red curve signifies the hot gas convective heat transfer area of the boundary node, the green dashed curve represents the outer and inner conductive heat transfer areas of *Node N*, the blue line denotes the cooling area of *Node N*, and the purple and yellow areas correspond to the volume and mass of the boundary node and internal node, respectively.

The mesh density has also been analyzed. Turbine disc mesh is chosen due to its complicated shape. The centre temperature change in the centre over time during a heat-up process is examined, as depicted in Fig. 7. It is observed that when the mesh density exceeded 200 nodes per meter (nodes/m), the deviations caused by node density are sufficiently small to be negligible. Therefore, in this study, a mesh density of 200 nodes/m is selected for application in the CVM.

B. Initial and Boundary Conditions

The initial temperature distribution in each component is determined based on the starting condition of the gas turbine transient manoeuvre. A steady-state heat transfer calculation is initiated to obtain the initial temperature distribution. Boundary conditions for each component is based on the HTC and fluid temperature. The HTC estimation is based [10]. Detailed equations are listed in Appendix A. The fluid temperature will be discussed here.

1) For the turbine blade, two boundaries need to be considered: the gas side wall and the internal cooling side wall. Regarding the gas side wall, the fluid temperature would be calculated using Eqs. (24),

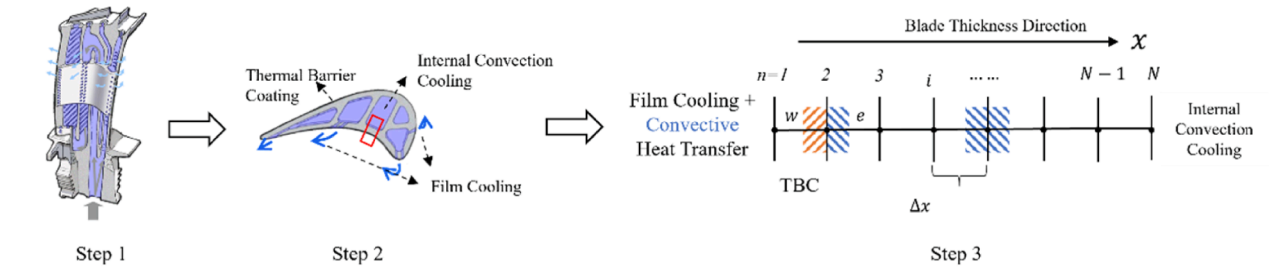

(a)

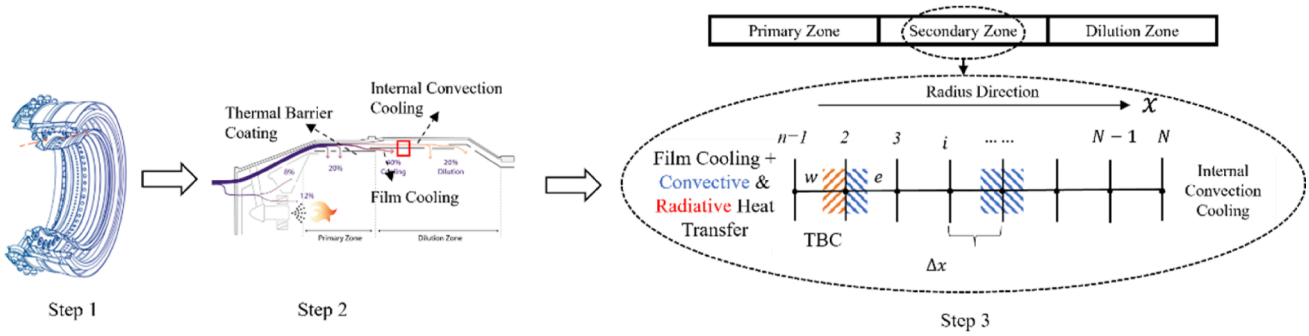

(b)

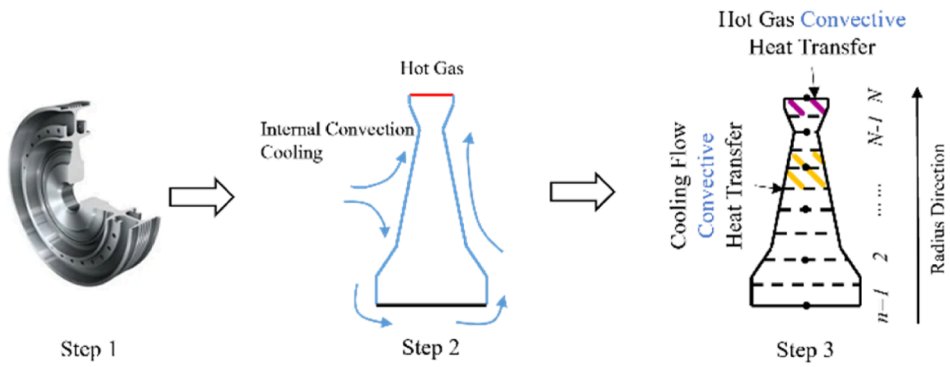

(c)

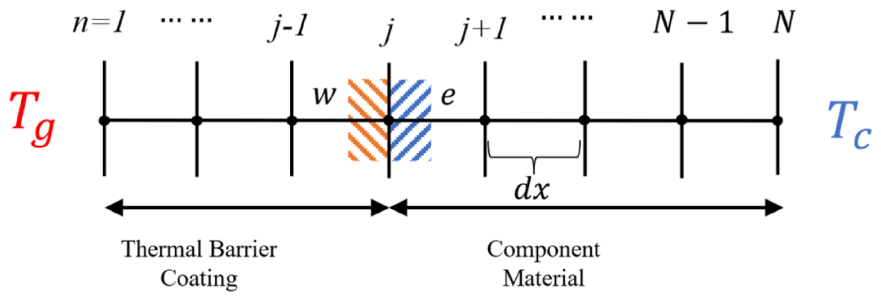

(d)

Fig. 5. Component geometry feature capture and mesh.

based on the gas temperature, the film cooling flow temperature and the cooling efficiency η_c. For the internal cooling side, the boundary fluid temperature is set as the cooling flow temperature.

$$T_{fluid} = T_g + \eta_c^* (T_c - T_g) \tag{24}$$

2) For the combustor flame tube, it is divided into different zones in the axial direction, each with its own temperature. Specifically, three combustor zones are considered: the primary zone, secondary zone, and dilution zone, as shown in Fig. 6 (b), Step 3. It is assumed that 40 % of the air will enter the primary zone for combustion, an additional 50 % of air will enter the secondary zone, and the remaining 10 % will enter the dilution zone. Each zone has two boundaries: the gas

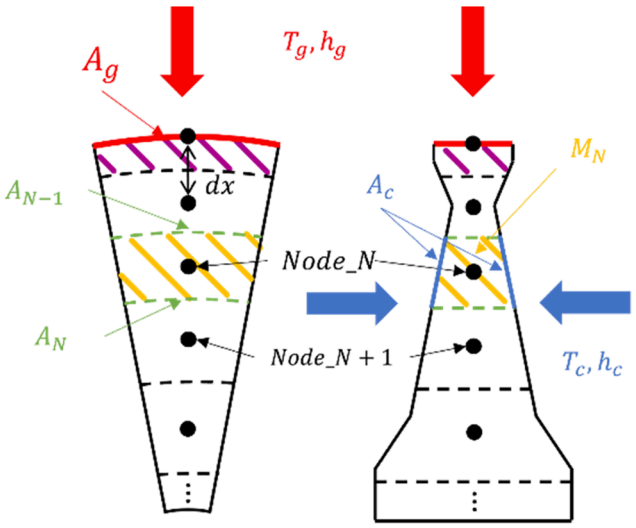

Fig. 6. Mesh outcome (turbine disc as an example).

side wall and the internal cooling side wall. For the gas side wall, the temperature profile is calculated first using Eqs. (25) [27], where *LHV* represents the lower heating value, *FAR* represents the fuel to air ratio, and η represents the efficiency. Then, the temperature profile is modified by the film cooling flow temperature using Eqs. (24). Additionally, radiative heat flow will be considered due to the extremely high temperature. For the internal cooling side, the boundary condition is set as the cooling flow temperature.

$$\boldsymbol{LHV \cdot FAR \cdot \eta_{burner}} = \boldsymbol{Cp \cdot (T_{out} - T_{in_{air}}) + Cp \cdot (T_{out} - T_{in_{fuel}})} \tag{25}$$

3) For the casing, two boundaries need to be considered: the gas side wall and the internal cooling side wall. For the gas side wall, the gas temperature will be set as the boundary condition. For the cooling wall, the cooling flow temperature will be set as the boundary condition.
4) For the compressor disc, only one boundary will be considered, which is the gas side wall. However, for the turbine disc, cavity cooling will be considered, and the cooling flow temperature will be set as the boundary condition.

C. Numerical Solving

The heat transfer calculation starts with the boundary convective heat transfer, followed by the inside conductive heat transfer. The general heat transfer equation for the CVM is shown in Eqs. (26), where λ is conductive coefficient, and x represents the distance.

$$\boldsymbol{\rho \cdot Cp \cdot \frac{\partial T}{\partial t} = \lambda \cdot \frac{\partial^2 T}{\partial x^2}} \tag{26}$$

The energy conservation law determines a node's temperature change, which states that the difference between the inlet and outlet heat flow causes an increase or decrease in the node temperature according to the material properties. Based on Eqs. (26) and an explicit finite difference scheme, the general node energy equation is shown in Eqs. (27)-(31):

$$\Phi_N = \Sigma\Phi_{conv} + \Sigma\Phi_{cond} + \Sigma\Phi_{radi} \tag{27}$$

$$\boldsymbol{\Phi_N = Cp \cdot M_N \cdot \frac{T_N^{i+1} - T_N^i}{dt}} \tag{28}$$

$$\boldsymbol{\Phi_{conv} = h_g \cdot A_g \cdot \left(T_g^i - T_N^i\right) + h_c \cdot A_c \cdot \left(T_c^i - T_N^i\right)} \tag{29}$$

$$\boldsymbol{\Phi_{cond} = \frac{\lambda}{dx} \cdot A_{N-1} \cdot \left(T_{N-1}^i - T_N^i\right) - \frac{\lambda}{dx} \cdot A_N \cdot \left(T_N^i - T_{N+1}^i\right)} \tag{30}$$

$$\boldsymbol{\Phi_{radi} = 0.5 \cdot \sigma \cdot A_{radi} \cdot (1 + \varepsilon_w) \cdot \varepsilon_g \cdot \left(T_g^i\right)^{1.5} \cdot \left(\left(T_g^i\right)^{2.5} - \left(T_N^i\right)^{2.5}\right)} \tag{31}$$

where subscript N represents node state, g represents gas flow, and c represents cooling flow, postscript i and $i+1$ represent transient calculation time step. σ represents the Stefan-Boltzmann constant, ε_w is the emissivity of the wall, and ε_g is the emissivity of the gas.

For the TBC, it is important to consider its effect on heat transfer during the meshing process. Fig. 6 (d) illustrates a 1-D mesh for that includes the TBC, shown in orange, and the component material, shown in blue. The position of node j is where the TBC and blade material are in contact. It is assumed that there is perfect thermal contact between the TBC and the blade material and no temperature difference within a single control volume. The energy equation for node j and the

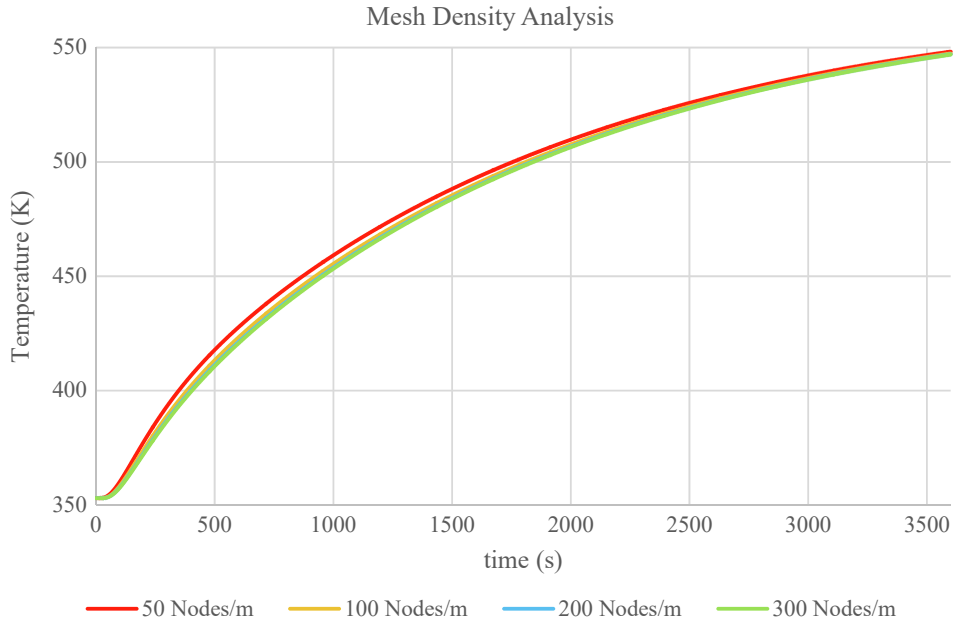

Fig. 7. Mesh density analysis.

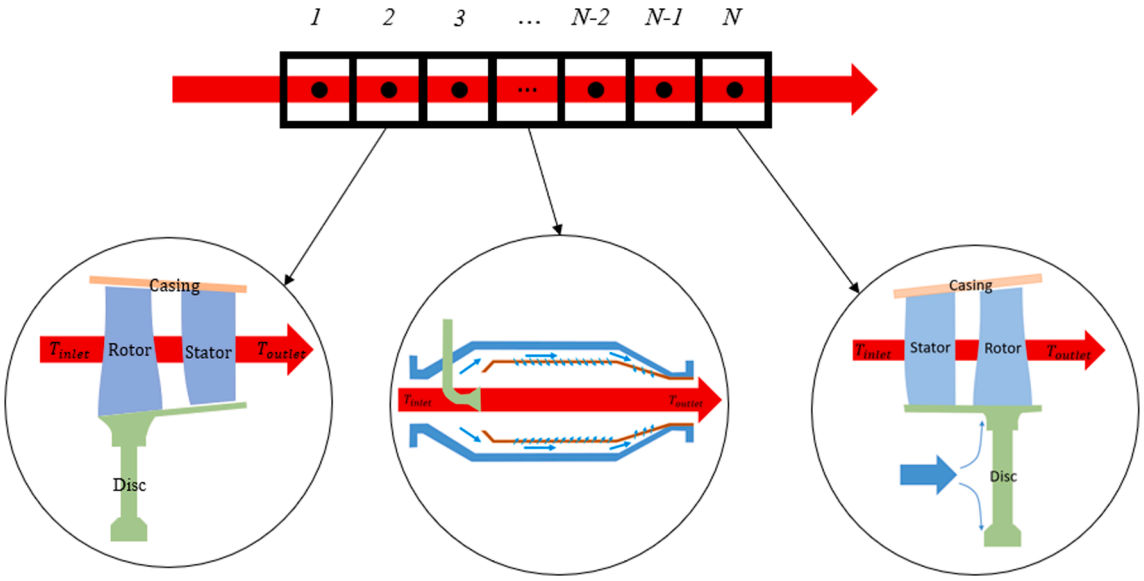

Fig. 8. Quasi-2D thermal network illustration.

Table 1
Summary of the quasi-2D thermal network.

Component	Heat Transfer Model		TBC	Film Cooling	Internal cooling Flow
	TDM	CVM			
Compressor Blade	√	×	×	×	×
Compressor Casing	√	×	×	×	×
Compressor Disc	×	√	×	×	×
Combustor Flame Tube	×	√	√	√	√
Turbine Blade	×	√	√	√	√
Turbine Casing	×	√	×	×	√
Turbine Disc	×	√	×	×	√

conductive heat transfer process in node j is shown in Eqs. (32) and Eqs. (33). Based on these equations, node j temperature at $i+1$ time step can be estimated.

$$\Phi_N = (\boldsymbol{Cp}_{tbc}\cdot\boldsymbol{M}_{tbc} + \boldsymbol{Cp}_b\cdot\boldsymbol{M}_b)\cdot\frac{\boldsymbol{T}_j^{i+1} - \boldsymbol{T}_j^i}{\boldsymbol{dt}} \tag{32}$$

$$\Phi_{cond} = \frac{\lambda_{tbc}}{\boldsymbol{dx}}\cdot\boldsymbol{A}_{j-1}\cdot\left(\boldsymbol{T}_{j-1}^i - \boldsymbol{T}_j^i\right) - \frac{\lambda_b}{\boldsymbol{dx}}\cdot\boldsymbol{A}_j\cdot\left(\boldsymbol{T}_j^i - \boldsymbol{T}_{j+1}^i\right) \tag{33}$$

2.1.3. Quasi-2D thermal network establishment

A quasi-2D thermal network is established along the gas flow direction, with each node having the ability to estimate the temperature distribution along the radial direction. Fig. 8 illustrates a quasi-2D thermal network established along the gas flow direction, where the red arrow represents the gas flow, and each black node represents one component stage or one combustion zone. Each node in the network estimates the temperature distribution along the radial direction and calculates heat soakage based on its own inlet and outlet condition. The calculated heat flow rate is then used to update the outlet condition, which becomes the inlet condition for the next node. This process includes three types of heat transfer: convective, conductive, and radiative heat transfer. Different heat transfer processes will be considered for different gas turbine components. The compressor blades and casing will only consider the convective heat transfer process. The compressor disc will consider convective and conductive heat transfer processes. The combustor flame tube will consider convective, conductive, and radiative heat transfer processes and the effects of film cooling and internal cooling flow. The turbine blade will consider two heat transfer processes: convective and conductive, considering TBC, film cooling, and internal cooling. The turbine disc will also consider two heat transfer processes: convective and conductive, with the consideration of cavity cooling. The turbine casing will consider two heat transfer processes: convective and conductive, considering the effect of internal cooling flow. A summary is listed in Table 1.

2.2. Component performance modification model

The estimated heat flow rate will affect the gas turbine component performance. For the combustor, the heat flow rate leads to adding or taking from the outlet station's enthalpy, changing the outlet temperature. For the compressor and turbine, it is assumed that part of the heat is transferred before the compression or expansion, and the rest is transferred afterwards. In this way, compression and expansion can still be calculated using (adiabatic) map data[11,13]. A user-defined ratio f is used to determine the part of heat that is transferred before the compression or expansion, as shown in Eqs. (34). Based on ratio f, the inlet temperature and outlet temperature of the compressor and turbine can be modified based on Eqs. (35) and (36) during the transient manoeuvre.

$$f = \frac{\boldsymbol{Q}_{pre}}{\boldsymbol{Q}_{total}} \tag{34}$$

$$\boldsymbol{T}_1^{'} = \boldsymbol{T}_1 + \frac{\boldsymbol{Q}_{pre}}{\boldsymbol{W}\cdot\boldsymbol{Cp}} \tag{35}$$

$$\boldsymbol{T}_2^{'} = \boldsymbol{T}_2 + \frac{(1-f)\boldsymbol{Q}_{total}}{\boldsymbol{W}\cdot\boldsymbol{Cp}} \tag{36}$$

2.3. Integration of heat soakage model

The mathematical models that accurately estimates the heat flow rate between the gas and engine components are developed above. However, the study of the heat soakage effect on gas turbine transient performance needs an accurate model and high-confidence platform to provide time-dependent engine working conditions. In this paper, the developed heat soakage has been integrated into TURBOMATCH (TM) to provide further insight into the heat soakage effect on gas turbine transient performance. TM is a Cranfield University in-house gas turbine performance code where pre-programmed units that called Bricks are

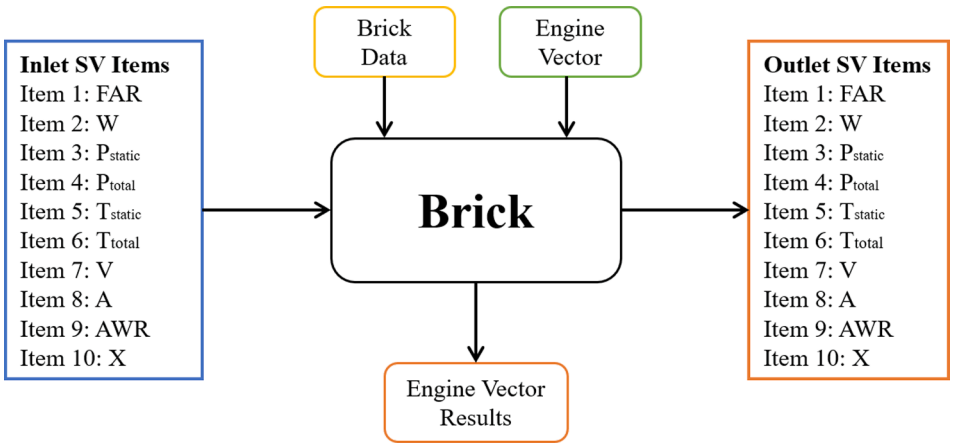

Fig. 9. TURBOMATCH brick structure.

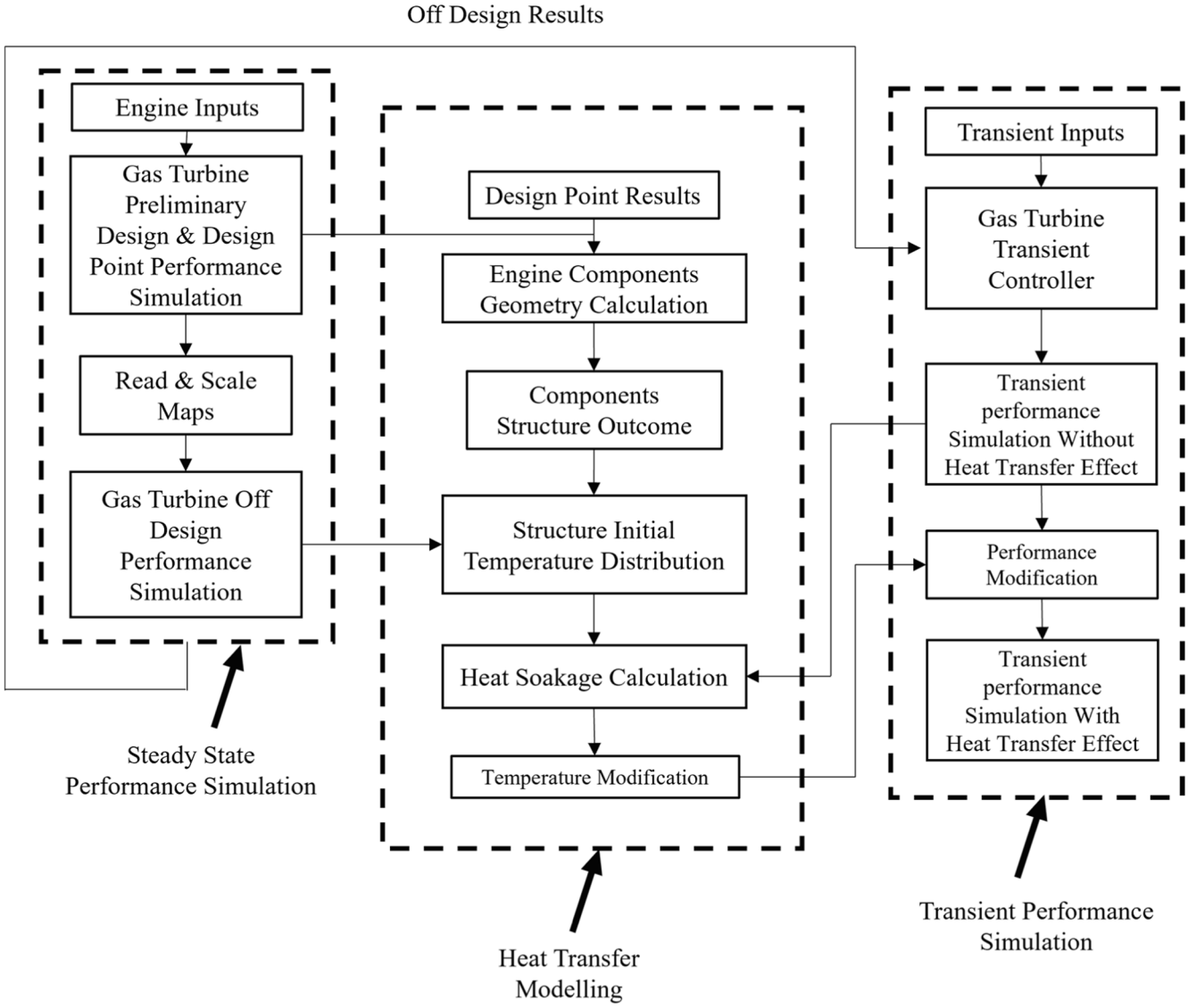

Fig. 10. Flow chart for the heat soakage calculation during transient.

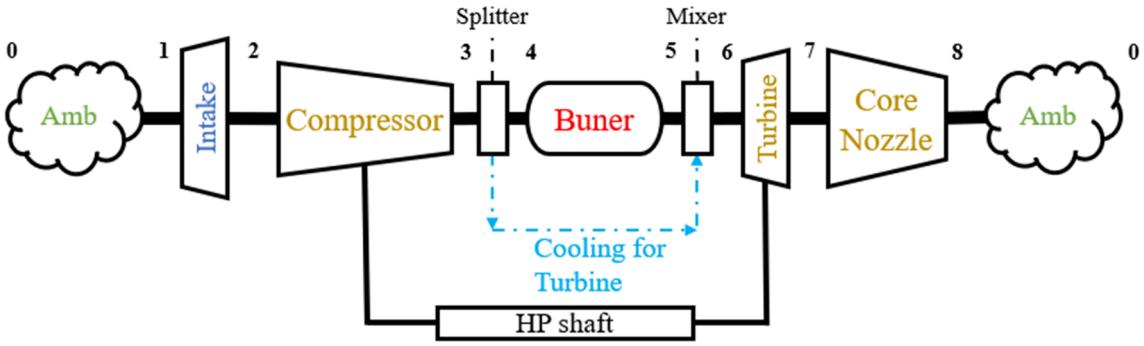

Fig. 11. Schematic of a one-spool turbojet engine.

Table 2
One spool turbojet engine parameters (Sea Level, Static, ISA condition).

Parameters	Value
Mass Flow (kg/s)	32
Compressor Pressure Ratio	12
Compressor Isentropic Efficiency	0.85
Combustor Outlet Temperature (K)	1450
Combustor Efficiency	0.99
Turbine Efficiency	0.85
Polar Moment of Inertia (kg*m^2)	4.05
Cooling Flow (%)	10
Engine Shaft Speed (rpm)	14,000
Thrust (kN)	26.73
SFC (g/(kN*s))	24.98

used for the simulation of gas turbine performance. Each Brick represents a particular component. Fig. 9 shows the Brick accompanying its input data and output data. In order to connect several Bricks to form an aeroengine as a whole, Station Vectors (SV) are applied as the inlet and outlet data of each Brick. Each SV consists of 10 different variable items as followed: Fuel-air ratio (FAR); Mass Flow (W); Static Pressure (P_static); Total Pressure (P_total); Static Temperature (T_static); Total Temperature (T_total); Velocity (V); Area (A); Water/Air Mass (WAR); Water phase (X). Users can define the input item of each Brick and the output item of that will be used as the input of the next sequential Brick. In this way, all individual Bricks can be linked with each other. More Information on the structure of TM is introduced by reference [28].

The calculation process is illustrated in Fig. 10. The design point gas turbine parameter will be used during the geometry identification that is discussed in Section 2.1.1. The last off-design condition will be set as the beginning of the transient manoeuvre and the initial condition of heat soakage estimation. During the transient, the heat soakage model will modify the component performance and find a new transient working point.

3. Heat soakage model validation

To validate the accuracy of the heat soakage model discussed in Section 2, two turbojet engine models are created. One model uses TM based on the developed heat soakage model, while the other uses Gas-Turb 12, a commercial software with the capability to simulate heat soakage effects. In this Section, the accuracy of the developed heat soakage model are discussed.

3.1. Turbojet engine model establishment

3.1.1. Engine structure and design point parameters

A one-spool turbojet engine is chosen as the simulation object. the structure of the gas turbine engine is shown in Fig. 11. The specific engine data and performance parameters are listed in Table 2.

3.1.2. Engine transient manoeuvre parameters

The transient simulation of the one gas turbine engine is also considered. For the control of transient operation, a fuel schedule is set as a function of time, and the CMF method is used to ensure consistency between the two software. Additionally, component performance maps used by both software are kept the same. The transient simulation assumed an acceleration from corrected rotational speed (CN) of 70 % to the maximum power at CN of 100 %. The fuel schedule, illustrated in Fig. 12, shows that it takes 1 s to reach the maximum power fuel flow from the fuel flow at CN of 70 %, and the entire transient manoeuvre lasts for 15 s.

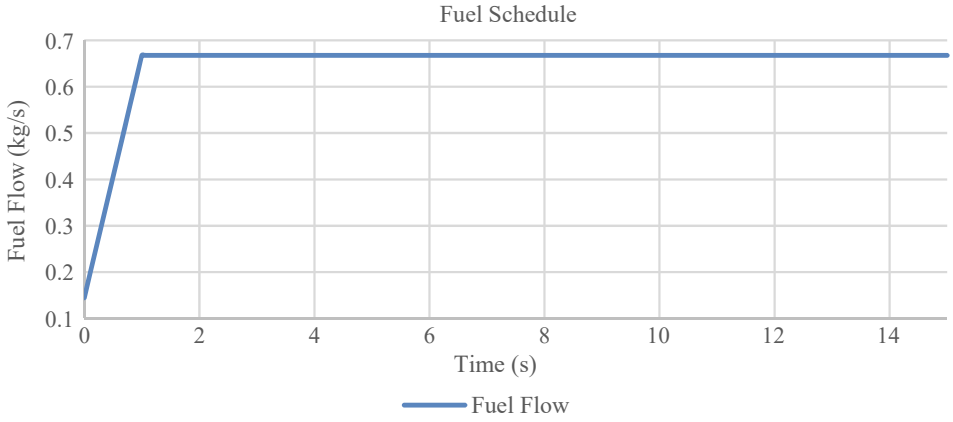

Fig. 12. Transient Fuel Schedule for Gas Turbine Transient Performance.

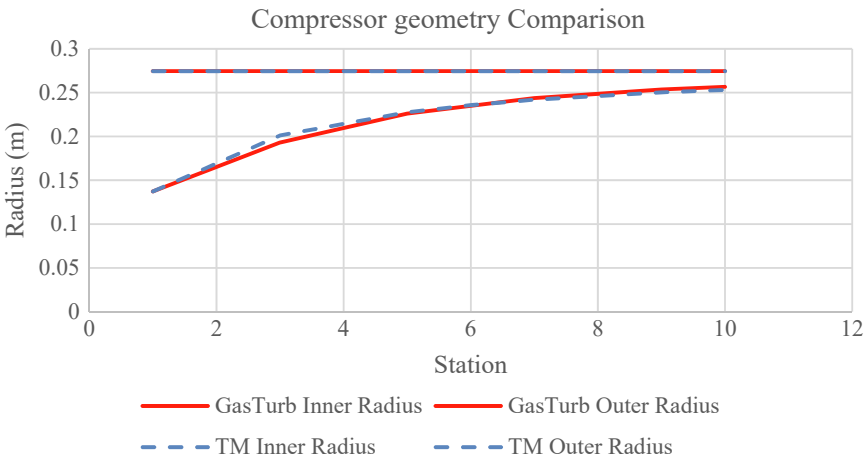

(a)

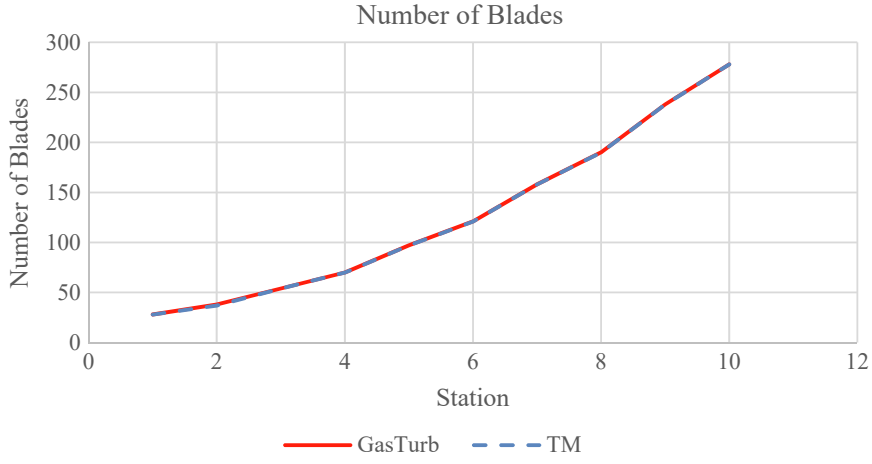

(b)

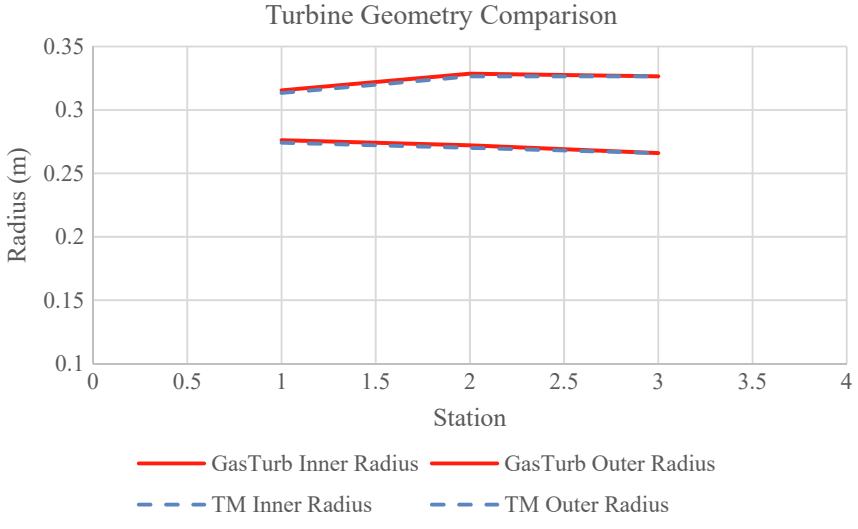

(c)

Fig. 13. Geometry comparison between TM and GasTurb.

Table 3
Wetted area and mass of component for two software.

	GasTurb	TM	Difference (%)
COMPRE Blade Mass	53.87 (kg)	53.79 (kg)	−0.14
COMPRE Blade Area	4.855 (m^2)	5.101 (m^2)	4.82
COMPRE Casing Mass	13.28 (kg)	13.27 (kg)	−0.06
COMPRE Casing Area	1.055 (m^2)	1.048 (m^2)	−0.71
COMPRE Disc Mass	43.47 (kg)	42.34 (kg)	−2.60
COMPRE Disc Area	0.257 (m^2)	0.256 (m^2)	−0.08
COMBUSTOR Can Mass	33.34 (kg)	33.54 (kg)	0.6
COMBUSTOR Can Area	1.667 (m^2)	1.687 (m^2)	1.21
TURBIN Blade Mass	10.93 (kg)	10.93 (kg)	−0.01
TURBIN Blade Area	1.041 (m^2)	1.046 (m^2)	0.55
TURBIN Casing Mass	4.333(kg)	4.246 (kg)	−2.00
TURBIN Casing Area	0.108 (m^2)	0.106 (m^2)	−2.00
TURBIN Disc Mass	23.19 (kg)	22.83 (kg)	−1.55
TURBIN Disc Area	0.045 (m^2)	0.044 (m^2)	−2.99

3.2. Quasi-2D thermal network validation

3.2.1. Components geometry identification validation

Before simulating the transient manoeuvre with heat soakage, it is crucial to ensure that the same heat transfer process is used, which requires the gas turbine model to have the same geometry. Based on the geometry identification outcome, the maximum difference between both software related to the compressor's inner radius is 4.3 %, and the difference in blade number is only 1, occurring at stator 1. For the turbine, the maximum difference for geometry is 1.3 % and there is no difference in blade number. The design outcomes by GasTurb and TM are illustrated in Fig. 13. These differences fall within the tolerance, indicating that the preliminary design accuracy is sufficient. To ensure consistency, the wetted area and mass of each component are also compared. While the compressor is divided into stages, ensuring that each stage's mass and wetted area are similar is challenging. Therefore, the component's total mass and wetted area are compared to keep both software at the same geometrical characteristics. The detailed data are presented in Table 3. The highest difference is found in compressor blade mass, which is overestimated by 4.82 %. With the difference limited to within 5 %, the structural outcome is reasonably good for the current study.

3.2.2. Component heat flow rate estimation validation

The transient manoeuvre discussed in Section 3.1.2 is applied to both TM and GasTurb. As GasTurb's heat soakage model doesn't include cooling technologies and the combustor temperature profile described above, the boundary conditions of the quasi-2D thermal network are modified for the GasTurb model: the film cooling efficiency is set to 0; the internal cooling temperature is set to the gas temperature; the TBC thickness is set to 0; metal thermal conductivity is set to 0; and radiative heat transfer is removed. Additionally, the combustor temperature profile is set as the mean combustor inlet and outlet temperature. With the above set-up, the heat transfer process aligns with that of GasTurb.

A comparison of the heat flow rate in each engine component over time between TM and GasTurb is presented in Fig. 14, showing good agreement between the two software. The maximum heat flow rate differences for the compressor, combustor, and turbine are −5.88 %, 7.94 %, and −3.08 %, respectively.

Combined with the geometry identification outcome, the quasi-2D thermal network has been validated and demonstrate satisfactory performance for the current study.

3.3. Component performance modification model validation

Based on the heat flow rate calculated in Section 3.2.2, the transient performances of the gas turbine are compared. A good agreement is observed under both conditions, without heat soakage and with heat soakage. The comparison of CN, compressor pressure ratio, and exhaust gas temperature are illustrated in Fig. 15. The solid lines represent the condition without considering heat soakage, while the dashed lines represent the condition with the consideration of heat soakage.

For CN, the maximum difference observed is 0.57 % at 1.45 s in the transient condition and 0.411 % at 1.3 s in the heat soakage condition. The maximum differences for the compressor pressure ratio are 0.065 in the transient condition and 0.073 in the heat soakage condition, both controlled within 0.7 %. The maximum difference for the exhaust gas temperature is 12.25 K in the transient condition and 23.37 K in the heat soakage condition, limited to 2.5 %. Based on the above discussion, the engine component performance modification method has been validated and demonstrate satisfactory performance for the current study.

4. Parametric study and analysis

In this section, the effect coming from combustor temperature profile, different cooling technologies and TBC on heat flow rate estimation will be discussed. Also, the change in gas turbine transient performance will be compared.

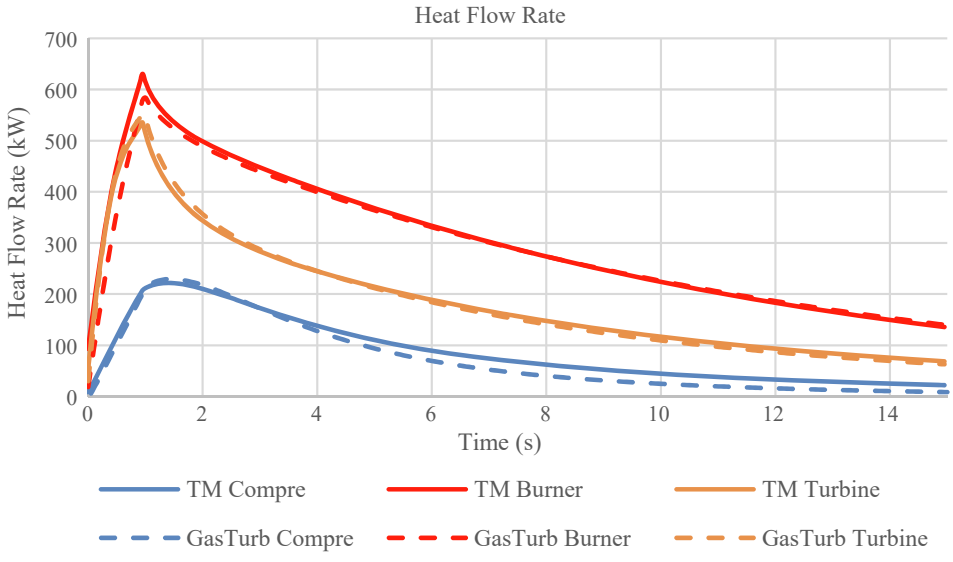

Fig. 14. Heat flow rate comparison between TM and GasTurb.

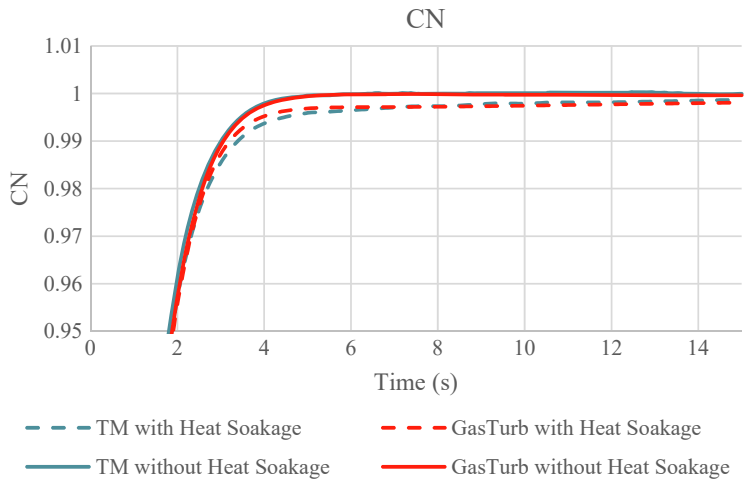

(a)

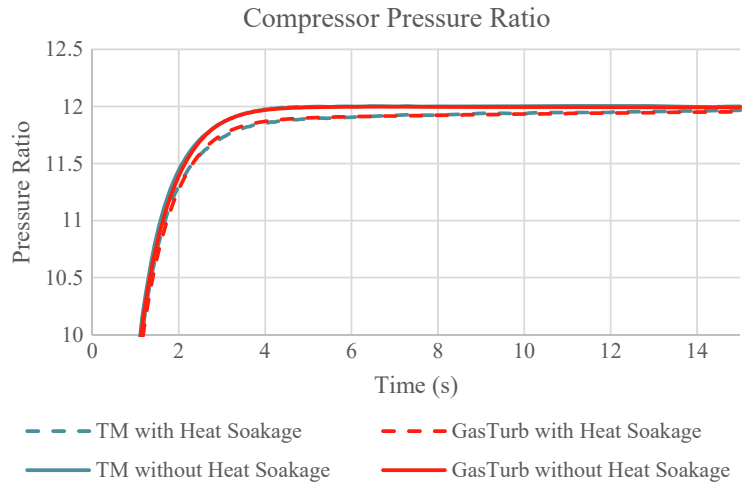

(b)

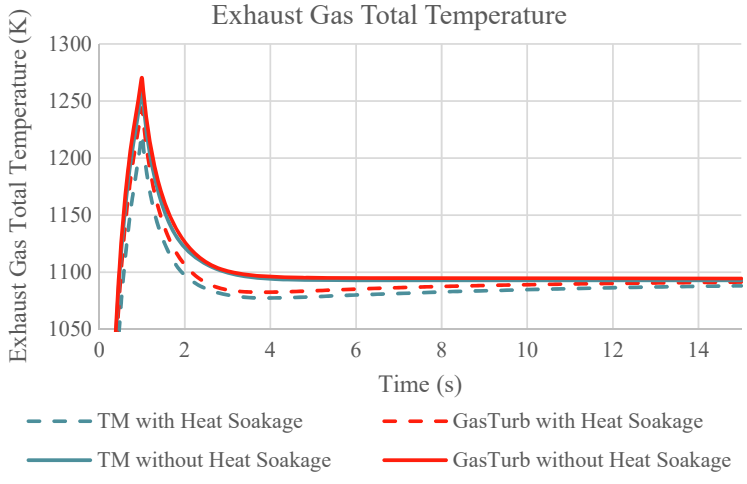

(c)

Fig. 15. Gas turbine transient performance comparison between TM and GasTurb with and without heat soakage effect.

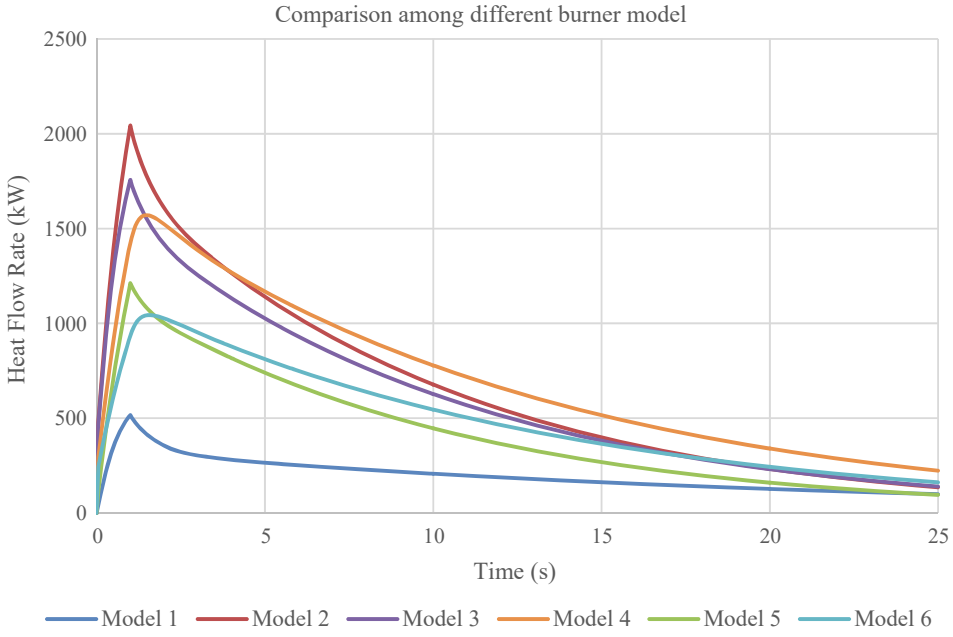

Fig. 16. Combustor temperature profile distribution and film cooling effect on heat transfer process.

4.1. Effect of combustor temperature profile and cooling technologies on heat flow rate

The simulation and comparison of the combustor temperature profile and different cooling technologies are investigated. The heat flow rate estimations of the combustor are estimated using six models:

Model 1: LPM based model;
Model 2: Quasi-2D thermal network based model; No cooling technologies; Considering combustor temperature profile;
Model 3: Quasi-2D thermal network based model; Only consider internal cooling; Considering combustor temperature profile;
Model 4: Quasi-2D thermal network based model; Considering internal cooling and TBC; Considering combustor temperature profile;
Model 5: Quasi-2D thermal network based model; Considering internal cooling and Film Cooling; Considering combustor temperature profile;
Model 6: Quasi-2D thermal network based model; Considering internal cooling, Film Cooling, and TBC; Considering combustor temperature profile.

The estimated heat flow rate values based on these models are illustrated in Fig. 16. A noticeable increase in heat flow rate is observed when comparing the results of the Model 1 and Model 2. During the acceleration, the Model 2′s peak heat flow rate value is approximately four times that of Model 1. This significant increase in heat flow rate can be attributed to the high temperatures in the primary and secondary zones, leading to a larger temperature difference and subsequent heat flow rate. By implementing the internal cooling, the heat flow rate of Model 3 is 14 % lower than Model 2. An additional reduction of 9 % heat flow rate is found when adding TBC (Model 4). Implementing film cooling and internal cooling technology proves to be highly effective in reducing the heat flow rate. With a cooling efficiency set at 0.45 and the cooling temperature based on the combustor's inlet temperature, the

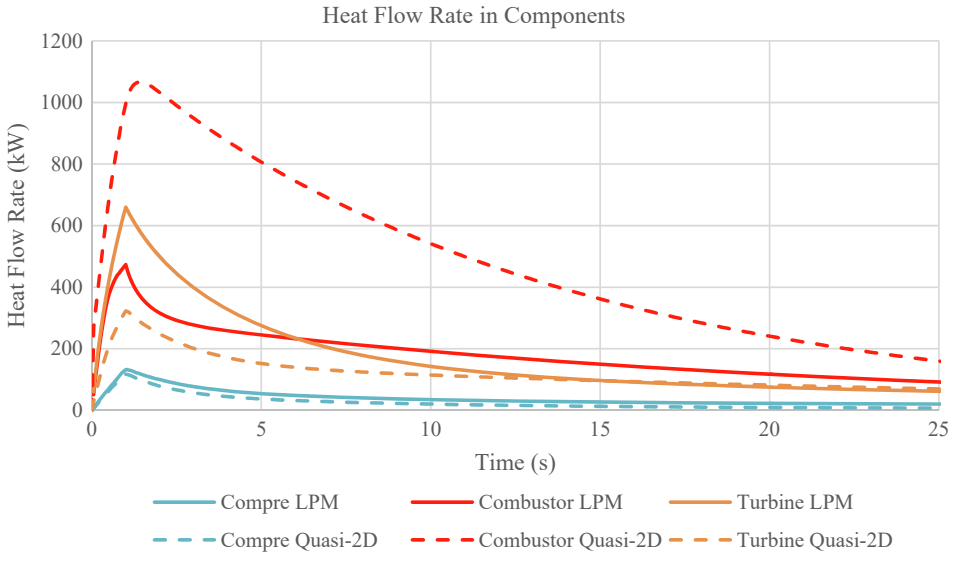

Fig. 17. Heat flow rate comparison between LPM based heat soakage model and quasi-2D thermal network based heat soakage model.

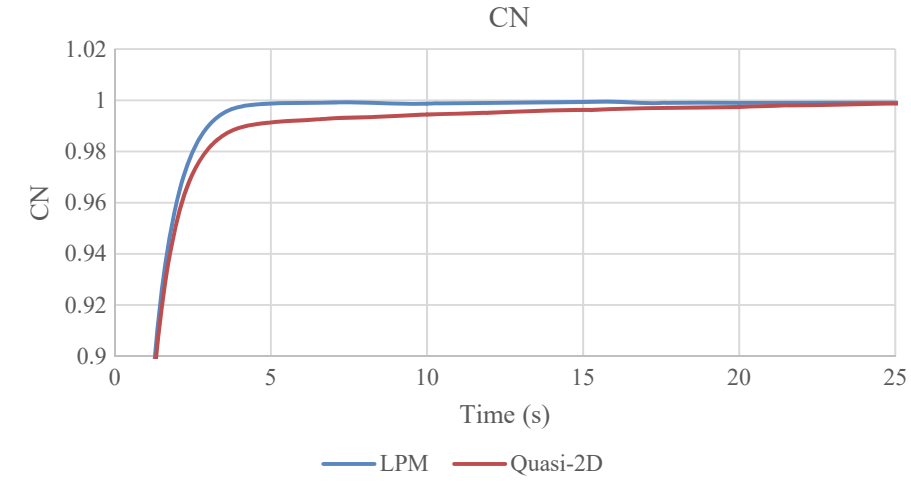

(a)

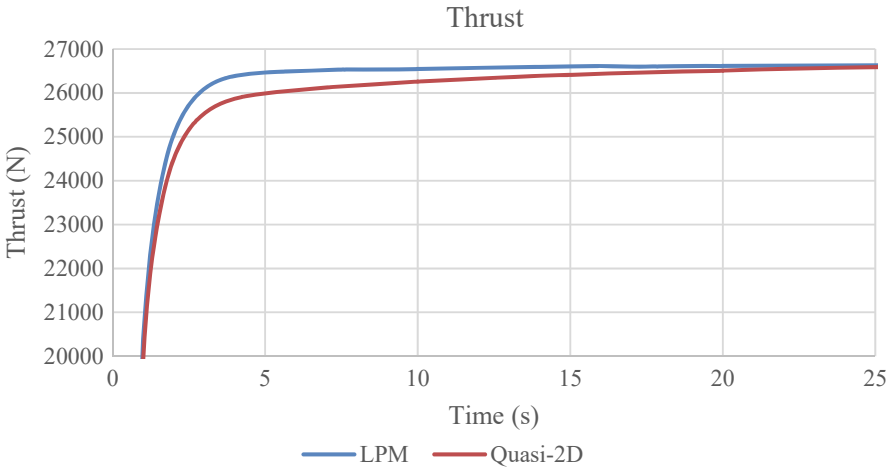

(b)

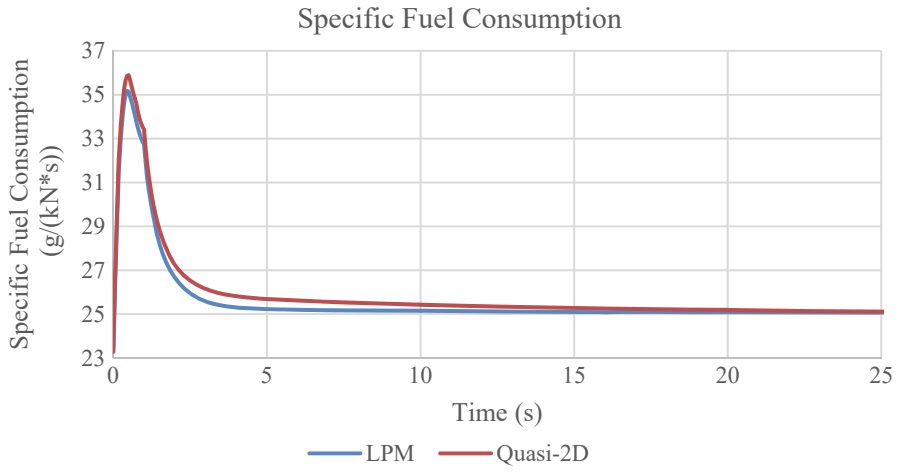

(c)

Fig. 18. Transient performance comparison between LPM based heat soakage model and quasi-2D thermal network based heat soakage model.

simulation shows a 40 % decrease in peak heat flow rate compared to Model 1. However, the heat flow rate is still 2.3 times higher than that of the Model 1. The application of TBC also contributes to reducing the heat flow rate (as shown in Model 6), owing to its low thermal conductivity. It is important to note that TBC also slows down the heat transfer process and results in a smaller temperature gradient. When film cooling, internal cooling and TBC are combined, a further reduction in heat flow rate is observed (48.97 %). Nevertheless, the heat flow rate is still twice as high as that of Model 1. Based on these findings, it becomes evident that considering the combustor temperature profile and incorporating cooling technologies are crucial aspects in heat soakage analysis. Neglecting these factors may lead to inaccurate assessments of heat soakage within the gas turbine components.

4.2. Heat flow rate variation effect on gas turbine transient performance

The variation in component heat flow rate directly impacts the gas turbine's transient performance. To evaluate this effect, a comprehensive comparison between LPM based heat soakage model and the proposed heat soakage model has been conducted, focusing on their respective influences on gas turbine transient performance. The engine geometry and transient manoeuvre remain consistent with the discussions presented in Section 3.1. The heat soakage model for compressor and turbine follows the setting in Table 1. And model 6 discussed in Section 4.1 is applied to the combustor.

The trend of heat flow rate in the compressor does not exhibit significant differences between the models. However, in the disc's radial direction, thermal resistance leads to a slightly lower heat flow rate. A remarkable increase is observed in the heat flow rate of the combustor. Compared to the LPM model, a substantial 150.5 % increase is identified. Nonetheless, due to the implementation of TBC and film cooling, the heat flow rate in the turbine experiences a reduction of 50.15 %. The estimation of heat flow rate based on two models is presented in Fig. 17.

The comparisons of transient performance are depicted in Fig. 18. It is evident that a delay is observed in the rate of increase of the shaft CN (Fig. 18 (a)). The maximum difference between two models is −0.89 %. Additionally, if we consider CN = 0.995 as the indicator of the completion of the transient manoeuvre, the LPM model achieves this point in 3.45 s, whereas the proposed heat soakage model requires 11.5 s. Therefore, the acceleration time under the proposed heat soakage model is extended by 8 s, nearly quadruple that of the LPM based heat soakage model. The choice of heat soakage model also affects the thrust during the transient manoeuvre. When the proposed heat soakage model is selected, there is a 2.24 % decrease in thrust compared to the LPM based heat soakage model, as shown in Fig. 18 (b). Furthermore, due to the decrease in thrust, the specific fuel consumption (SFC) during the gas turbine transient manoeuvre increases by 2.29 %, as depicted in Fig. 18 (c).

Based on the discussion, the proposed heat soakage model can estimate more realistically the heat transfer during engine transients compared to the conventional LPM based heat soakage model. The selection of the heat soakage model yields distinct outcomes in heat flow rate estimation, thereby influencing the gas turbine's transient performance accordingly. By incorporating the combustor temperature profile and cooling technologies, a more accurate representation of the heat transfer process is achieved, resulting in a notable variation in heat flow rate estimation. The observed disparities in gas turbine transient performance emphasize the significance of including these features in contemporary heat soakage models. The novel heat soakage model offers an improved understanding of heat transfer dynamics and its impact on engine performance during transients.

5. Conclusion

A novel quasi-2D thermal network based heat soakage model has been developed and integrated into the TM, an in-house gas turbine simulation software at Cranfield, to estimate heat soakage during transient manoeuvrees accurately. This thermal network incorporates several advancements, including consideration of component internal thermal resistance, consideration of axial temperature distribution in the combustor, and accounting for film cooling, TBC, and internal cooling. The accuracy of proposed heat soakage model is validated against the results obtained from GasTurb, ensuring a difference within 1.2 %. A further investigation is launched by comparing the LPM based heat soakage model with the proposed heat soakage model. The findings are listed below:

1. The combustor temperature profile model can offer a more realistic heat flow rate estimation in the combustor. The findings revealed a significant increase (four times that of the LPM based model) in heat flow rate within the combustor due to the high temperature in the primary zone and secondary zone.
2. Cooling technologies implementation effectively decreases the rate at which heat flows. In comparison to the combustor temperature profile model: internal cooling reduces the heat flow rate by 14 %; internal cooling and TBC reduce the heat flow by 23 %; film cooling and internal cooling reduces the heat flow rate by 40 %; film cooling, internal cooling and TBC reduces it by 48.97 %. However, even with these measures, the heat flow rate still remains twice as high as the LPM model.
3. The proposed heat soakage model provided a more realistic estimation of heat soakage effect, further reducing the gas turbine's transient response. During the acceleration process, there is a 0.89 % decrease in corrected rotational speed, and the corrected rotational speed increase time is extended by 8 s. Additionally, the thrust is reduced by 2.24 %, and SFC is increased by 2.29 %. The outcome reveals the importance of considering combustor temperature profile, film cooling and TBC in heat soakage analysis.

The proposed heat soakage model demonstrated its capability to simulate the heat soakage effect in greater detail during gas turbine transients. These results highlight the promising potential of the heat soakage model and its applicability to other gas turbine engines.

Declaration of competing interest

The authors declare that they have no known competing financial interests or personal relationships that could have appeared to influence the work reported in this paper.

Data availability

No data was used for the research described in the article.

Appendix A

During the heat soakage simulation, gas and metal thermal properties will variate due to the temperature change.
The calculation of dry air *Cp* is based on the model provided in Walsh and Fletcher [6] according to which:

Table 4
thermal properties of superalloy Inconel 718.

T, K	λ, W/(m K)	Cp, J/(g K)
298	9.94	0.425
400	11.59	0.447
500	13.24	0.468
600	14.91	0.489
700	16.61	0.510
800	18.34	0.531
1100	22.72	0.635
1200	23.61	0.635
1300	24.47	0.635
1400	25.32	0.634

$$\boldsymbol{Cp} = \boldsymbol{A}_0 + \boldsymbol{A}_1\boldsymbol{TZ} + \boldsymbol{A}_2\boldsymbol{TZ}^2 + \boldsymbol{A}_3\boldsymbol{TZ}^3 + \boldsymbol{A}_4\boldsymbol{TZ}^4 + \boldsymbol{A}_5\boldsymbol{TZ}^5 + \boldsymbol{A}_6\boldsymbol{TZ}^6 + \boldsymbol{A}_7\boldsymbol{TZ}^7 + \boldsymbol{A}_8\boldsymbol{TZ}^8 \tag{37}$$

where TZ = T/1000 and A are constants for dry air as shown below:

A_0	0.992313
A_1	0.236688
A_2	−1.852148
A_3	6.083152
A_4	−8.893933
A_5	7.097112
A_6	−3.234725
A_7	0.794571
A_8	−0.081873

The material chosen is superalloy Inconel 718, which is widely applied in modern manufacturing for the aerospace and nuclear industries. The material thermal properties are obtained from experimental data as shown in Table 4. [29].

When calculating the heat transfer coefficient for compressor blades, casing and disc, it is assumed that the flow starts with laminar flow and then transfer into turbulence flow. The weighted average method is applied during this process. For laminar flow, the heat transfer coefficient is estimated by Eqs. (38). For turbulence flow, the heat transfer coefficient is estimated by Eqs. (39). The average heat transfer coefficient is estimated by Eqs. (40), where f is the average coefficient. For turbine and combustor, it is assumed the flow is turbulence flow and Eqs. (41) is used for heat transfer coefficient estimation.

$$\boldsymbol{N_u} = \frac{\boldsymbol{h_L}\cdot\boldsymbol{\lambda}}{\boldsymbol{L}} = 0.664(\boldsymbol{Re})^{0.5}(\boldsymbol{Pr})^{0.333} \tag{38}$$

$$\boldsymbol{N_u} = \frac{\boldsymbol{h_T}\cdot\boldsymbol{\lambda}}{\boldsymbol{L}} = 0.037(\boldsymbol{Re})^{0.8}(\boldsymbol{Pr})^{0.333} \tag{39}$$

$$\boldsymbol{h_{ave}} = \boldsymbol{f}\cdot\boldsymbol{h_L} + (1-\boldsymbol{f})\cdot\boldsymbol{h_T} \tag{40}$$

$$\boldsymbol{N_u} = \frac{\boldsymbol{h}\cdot\boldsymbol{\lambda}}{\boldsymbol{L}} = 0.235(\boldsymbol{Re})^{0.64} \tag{41}$$

References

[1] V.L. Larrowe, M.M. Spencer, M. Tribus, A dynamic performance computer for gas-turbine engines, J. Fluids Eng. 79 (7) (1957) 1707–1714, https://doi.org/10.1115/1.4013457.

[2] A.J. Fawke, H.I.H. Saravanamuttoo, Experimental Investigation of Methods for Improving the Dynamic Response of a Twin-Spool Turbojet Engine, J. Eng. Power 93 (4) (1971) 418–424, https://doi.org/10.1115/1.3445601.

[3] Y.G. Li, N.R.L. Maccallum, P. Pilidis, Pressure waves in volume effect in gas-turbine transient-performance models, J. Propuls. Power 17 (3) (May 2001) 706–710, https://doi.org/10.2514/2.5799.

[4] Z. Li, "Aircraft engine transient performance modelling with heat soakage effects, Cranfield University", 2019. Ph.D thesis.

[5] J. Kurzke, H. Ian, Propulsion and power : an exploration of gas turbine performance modeling, First Ed. Springer (2018).

[6] P.P. Walsh, P. Fletcher, Gas turbine performance, Second ed., Oxford Blackwell Science, 2004.

[7] Y. Yang, T. Nikolaidis, S. Jafari, P. Pilidis, "Gas turbine engine transient performance and heat transfer effect modelling: A comprehensive review, research challenges, and exploring the future," *Appl. Therm. Eng.* vol. 236(PA) p. 121523 (2024) Doi: 10.1016/j.applthermaleng.2023.121523.

[8] N. R. L. MACCALLUM, "Effect of 'Bulk' Heat Transfers in Aircraft Gas Turbines on Compressor Surge Margins.," 1973. https://www.scopus.com/record/display.uri?eid=2-s2.0-85042249153&origin=resultslist&sort=r-f&src=s&sid=4335a063ca0ba22ba29818a52c94fa0f&sot=aut&sdt=a&sl=17&s=AU-ID%286701497875%29&relpos=9&citeCnt=0&searchTerm= (accessed 14 March 2023).

[9] S. KHALID and R. HEARNE, "Enhancing dynamic model fidelity for improved prediction of turbofanengine transient performance," Jun. 1980, 10.2514/6.1980-1083.

[10] T. Qiuye, J. Rui, X. Xuan, Z. Heng, Y. Hongming, Effects of heat soakage on transient performance of gas turbine engine, J. Aerosp Power 32 (3) (2017) 630–636, https://doi.org/10.13224/j.cnki.jasp.2017.03.015.

[11] M. Vieweg, F. Wolters, R.-G. Becker, "Comparison of a Heat Soakage Model With Turbofan Transient Engine Data", in Volume 1: Aircraft Engine; Fans and Blowers, Marine; Honors and Awards 1 (Jun. 2017) 1–12, https://doi.org/10.1115/GT2017-63461.

[12] Z. Zhili, L. Kuo, Analysis of heat transfer impacting on gas turbine engine transients, J. Propuls. Technol. 17 (3) (1996) 10–15.

[13] W.P.J. Visser, I.D. Dountchev, "Modeling thermal effects on performance of small gas turbines", in Volume 1: Aircraft Engine; Fans and blowers, Marine 1 (2015) 1–12, https://doi.org/10.1115/GT2015-42744.

[14] M. Vieweg, C. Klein, S. Reitenbach, F. Wolters, and R. G. Becker, "Coupling of predesign and performance tools for transient aircraft engine analyses," 2018.

[15] P.H. Naylor, "Gas turbine transient performance: heat soakage modelling, Cranfield University", 2004. Ph.D thesis.

[16] J.A. Kypuros, K.J. Melcher, A reduced model for prediction of thermal and rotational effects on turbine tip clearance, NASA Technical Memorandum, NASA/TM-2003-212226 (2003).

[17] J.A. Kypuros, R. Colson, A. Muiioz, Improved temperature dynamic model of turbine subcomponents for facilitation of generalized tip clearance control, NASA NAG3-2857 (2004).

[18] J. W. Chapman, T.-H. Guo, J. L. Kratz, and J. S. Litt, "Integrated Turbine Tip Clearance and Gas Turbine Engine Simulation," in: *52nd AIAA/SAE/ASEE Joint Propulsion Conference*, Jul. 2016, pp. 1–16, 10.2514/6.2016-5047.
[19] J. L. Kratz, D. E. Culley, and J. W. Chapman, "Approximation of Engine Casing Temperature Constraints for Casing Mounted Electronics," in: *52nd AIAA/SAE/ASEE Joint Propulsion Conference*, Jul. 2016, pp. 1–23, 10.2514/6.2016-4858.
[20] F. Chen, Y. Chen, K. Song, and Y. Li, "Study on the Influence of Heat Transfer Effect on Performance Simulation of Engine Transition State," in: *2019 IEEE 10th International Conference on Mechanical and Aerospace Engineering (ICMAE)*, Jul. 2019, pp. 443–448, 10.1109/ICMAE.2019.8880972.
[21] Z.-J. Li, Y.-G. Li, T. Korakianitis, "Gas Turbine Transient Performance Simulation With Simplified Heat Soakage Model", in Volume 5: Controls, Diagnostics, and Instrumentation; Cycle Innovations, *Cycle Innovations: Energy Storage* 2020 (5) (1968) 1–12, https://doi.org/10.1115/GT2020-14484.
[22] A. Ferrand, M. Bellenoue, Y. Bertin, R. Cirligeanu, P. Marconi, F. Mercier-Calvairac, "High Fidelity Modeling of the Acceleration of a Turboshaft Engine During a Restart", in Volume 1: Aircraft Engine, *Fans and Blowers; Marine*, Jun. 1 (2018), https://doi.org/10.1115/GT2018-76654.
[23] H.I.H. Saravanamuttoo, G.F.C. Rogers, H. Cohen, Gas turbine theory, Sixth ed., Pearson Prentice Hall, 2009.
[24] Z. Li, Y.G. Li, S. Sampath, Aeroengine transient performance simulation integrated with generic heat soakage and tip clearance model, Aeronaut. J. (2022) 1–23, https://doi.org/10.1017/aer.2022.15.
[25] A.H. Lefebvre, D.R. Ballal, Gas turbine combustion, CRC Press, 2010.
[26] H. SHENG, T. LIU, Y. ZHAO, Q. CHEN, B. YIN, and R. HUANG, "New model-based method for aero-engine turbine blade tip clearance measurement," *Chinese J. Aeronaut.*, no. September, Sep. 2022, 10.1016/j.cja.2022.09.012.
[27] C.P. Mark, A. Selwyn, Design and analysis of annular combustion chamber of a low bypass turbofan engine in a jet trainer aircraft, Propuls. Power Res. 5 (2) (2016) 97–107, https://doi.org/10.1016/j.jppr.2016.04.001.
[28] J. Janikovic, "Gas turbine transient performance modeling for engine flight path cycle analysis, Cranfield University", 2010. Ph.D thesis.
[29] A.S. Agazhanov, D.A. Samoshkin, Y.M. Kozlovskii, Thermophysical properties of Inconel 718 alloy, J. Phys. Conf. Ser. 1382 (1) (2019) 012175, https://doi.org/10.1088/1742-6596/1382/1/012175.

2024-01-09

Quasi-2D thermal network based heat soakage model for gas turbine transient performance modification

Yang, Yimin

Elsevier

Yang Y, Nikolaidis T, Pilidis P. (2024) Quasi-2D thermal network based heat soakage model for gas turbine transient performance modification. Applied Thermal Engineering, Volume 241, March 2024, Article number 122340

https://doi.org/10.1016/j.applthermaleng.2024.122340